Simulated Effect of Vadose Infiltration on Water Levels in the Northern Guam Lens Aquifer

D.N. Contractor[1]
&
J.W. Jenson[2]

[1]*Department of Civil Engineering*
and Engineering Mechanics
University of Arizona
Tucson, AZ 85721

[2]*Water and Environmental Research Institute*
of the Western Pacific
University of Guam
Mangilao, GU 96923

Technical Report No. 90

Water & Environmental Research Institute
of the Western Pacific
University of Guam

November 1, 1999

The work reported here was supported by the Guam Hydrologic Survey Program of the Water & Environmental Research Institute, University of Guam. The content of this report does not necessarily reflect the views and policies of the Government of Guam, nor does the mention of trade names or commercial products constitute their endorsement by the Government of Guam.

Abstract

Regional-scale hydrology of the fresh water lens in the Northern Guam Lens Aquifer has been simulated in the past using a finite element, sharp interface computer model, SWIG2D. Systematic differences exist between observed and computed water levels. Computed seasonal peak water levels are higher, and the computed seasonal lows are lower than the respective observed levels. It is hypothesized that vadose storage must store a substantial amount of water during the wet season and release it gradually into the lens during the dry season. Flow through the vadose zone was simulated with a one-dimensional finite element, unsaturated flow program, UNSAT1D, in which the van Genuchten model is used to characterize unsaturated diffuse flow through the matrix of the vadose zone. An additional parameter (SINK) was added to the van Genuchten set to account for rapid infiltration down open pathways (fractures) associated with the closed depressions of the karst terrain. A global-optimization technique (Shuffled Complex Evolution or SCE-UA Method) was used to obtain the parameters that minimized the difference between simulated and observed water levels. Simulations incorporating the van Genuchten model were accomplished by combining the two programs, UNSAT1D and SWIG2D, into a single program. The sum-of-squared-errors (SSE) between computed and observed water levels in four observation wells was minimized using SCE-UA, reducing the arithmetically-averaged SSE of the four wells by 30% compared with the SSE obtained when the vadose zone was not modeled. These results suggest that vadose storage is significant. On the other hand, the fact that the best fit obtained with an optimum parameter set was able to reduce the SSE by no more than 30% suggests that additional phenomena have yet to be accounted for to more fully explain differences between simulated and observed well water levels.

Keywords: coastal, ground water models, Guam, karst Hydrology, vadose zone.

Contents

List of Figures

List of Tables

SIMULATED EFFECT OF VADOSE INFILTRATION ON WATER LEVELS IN THE NORTHERN GUAM LENS AQUIFER

Dinshaw N. Contractor[1] and John W. Jenson[2]

[1]*Department of Civil Engineering and Engineering Mechanics, University of Arizona*
Tucson, AZ 85721, USA

[2]*Water & Environmental Research Institute of the Western Pacific, University of Guam*
Mangilao, GU 96923, USA

1. Introduction

The Northern Guam Lens Aquifer (NGLA) provides 80% of Guam's potable water production of about 1.7 m^3s^{-1} (40 mgd) for its 150,000 permanent residents and over 1,000,000 tourists who visit the island annually. The economy of the island will demand increasingly more of this fundamental resource as the island's population and economy continue to grow. As limits to production are approached, understanding aquifer characteristics is imperative if the aquifer is to be managed properly to meet future demand and preserve water quality. The most comprehensive study of aquifer characteristics to date is still the Northern Guam Lens Study (NGLS), a three-year, $3.5M study administered by the Guam Environmental Protection Agency and completed in 1982. The NGLS produced several volumes and maps containing a large amount of empirical geologic and geophysical data, which still provide the baseline for current work (CDM, 1982). The results of the NGLS and subsequent work are summarized by Mink and Vacher (1997). Among the most important contributions of the NGLS was that it put in place an expanded hydrographic data collection program under which the US Geological Survey collects groundwater, tidal, and precipitation data on the aquifer. Data collection sites associated with the work reported here are shown in Figure 1.

An additional initiative of the NGLS was development of SWIG2D, a two-dimensional, finite element, dual-phase/sharp interface, Darcian-Dupuit model for studying saltwater intrusion vulnerability (Contractor, 1981; Contractor, 1983; Contractor *et al.*, 1981). The original program was subsequently modified to run on a personal computer (Contractor and Srivastava, 1990), and more recently modified so that anisotropic media could be modeled. In addition, a sparse-matrix, iterative equation solver (Kincaid *et al.*, 1997) has been added. Details of the model are summarized in the appendix.

These improvements have supported ongoing applications of SWIG2D to recent studies of the NGLA at the Water & Environmental Research Institute of the Western Pacific, University of Guam, aimed at exploiting the hydrographic data that have accumulated since 1982. A recent application of SWIG2D to simulate water levels in the aquifer over the 14-year record from 1982 through 1995 using refined estimates of recharge (Jocson, 1998; Jocson *et al.*, 1999) showed that for simulations in which all recharge in any given month is assumed to infiltrate to the phreatic zone within the same month, the amplitude (*i.e.*, (max - min) in a year) of each simulated

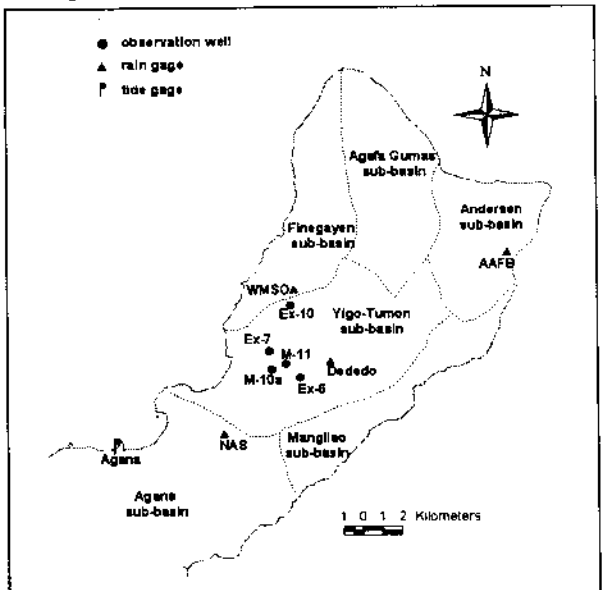

Figure 1. Map of northern Guam showing the sub-basins of the Northern Guam Lens Aquifer, the observation wells and other data collection sites referred to in this report. Domain of the model includes the entire Yigo-Tumon sub-basin and the most of the Finegayen sub-basin.

curve is consistently larger than the amplitude of the corresponding curve for the observed water levels (Figure 2). These systematic differences suggested that the vadose zone might store substantial rainfall excess (rainfall minus evapo-transpiration) during the peak inflows of the wet season, releasing the water gradually during the low inflows of the dry season. This paper reports on a modeling study conducted to evaluate this hypothesis by coupling a model of vadose infiltration to a SWIG2D-based model of phreatic groundwater dynamics (Jocson, 1998; Jocson *et al.*, 1999). The coupled model provides a means to determine the extent to which incorporating vadose processes into the model can reduce the differences between simulated and observed water levels. We describe here the implementation of the coupled model, as well as the results.

2. Hydrogeologic characteristics of northern Guam

The surface of Northern Guam is a gently sloping limestone plateau occupying about half of the island's area of 550 km^2 (212 $mi.^2$). The southern portion of the plateau rises from sea level to 60 meters while the northern portion has a maximum elevation of about 180 meters. Average annual rainfall is about 2.54 m (100 inches), about 70-80% of which falls during the wet season from July through December.

The NGLA is composed primarily of two permeable limestone formations, the Pliocene-Pleistocene Mariana Limestone, and the Miocene-Pliocene Barrigada Limestone (Tracey *et al.*, 1964). The Mariana Limestone was deposited as a shallow-water fringing and barrier reef, and is therefore thickest along the rim of the uplifted plateau. Inland, a lagoonal facies of the Mariana Limestone grades downward into the Barrigada Limestone, which is a deeper-water limestone of bank and off-reef detrital deposits. The Barrigada Limestone dominates the interior of the plateau and accounts for the greatest volume of the aquifer, especially the modern phreatic zone and the vadose zone of the island's interior. The basement beneath the limestone is a late Eocene-Oligocene submarine volcaniclastic deposit, the permeability of which is many orders of magnitude lower than the overlying limestone.

Mylroie and Vacher (1999) have proposed the term *eogenetic karst* to describe the system of landforms, secondary porosity, and hydrologic flow systems that develops in young island carbonate units, where post-depositional alteration has taken place exclusively in the realm of actively circulating ground water. Permeability increases as porosity is redistributed from primary to secondary porosity. Karstigenesis produces a dual-porosity aquifer in which dissolution-widened fractures are typically superimposed on a high-porosity matrix. The conductivity associated with each component is high, though variable, and can be orders of magnitude different from the other. On northern Guam, regional-scale hydraulic conductivity inferred from studies of tidal-signal attenuation in inland wells ranges from 1 to 6 km/day (Ayers and Clayshulte, 1984). Local values derived from pumping tests on the other hand, are typically on the order of 1 to 100 m/day. The contrast between these regional-scale and local conductivity values is consistent with the dual porosity model of island karst proposed by Vacher and Mylroie (submitted). Single-porosity Darcian models must therefore be applied with care to restrict them to appropriate scales and processes.

Previous applications of SWIG2D (Contractor, 1983; Contractor and Srivastava, 1990; Jocson, 1998; Jocson *et al.*, 1999) to the simulation of the dynamic behavior of the phreatic zone in the NGLA have shown that a Darcian-flow model can simulate regional-scale processes with characteristic times of a few weeks or more (*e.g.*, regional water table responses to monthly and seasonal-scale variations in sea level and precipitation). Regional-scale hydraulic conductivity values inferred from island-scale models, generally within 20% of 6 km/day, are consistent with the upper end of the range observed by Ayers and Clayshulte (1984) from their evaluation of tidal-signal attenuation in inland wells. Since the study reported here is similarly confined to regional-scale and long-term phenomena, the application of SWIG2D for modeling the phreatic dynamics of the coupled model was deemed appropriate.

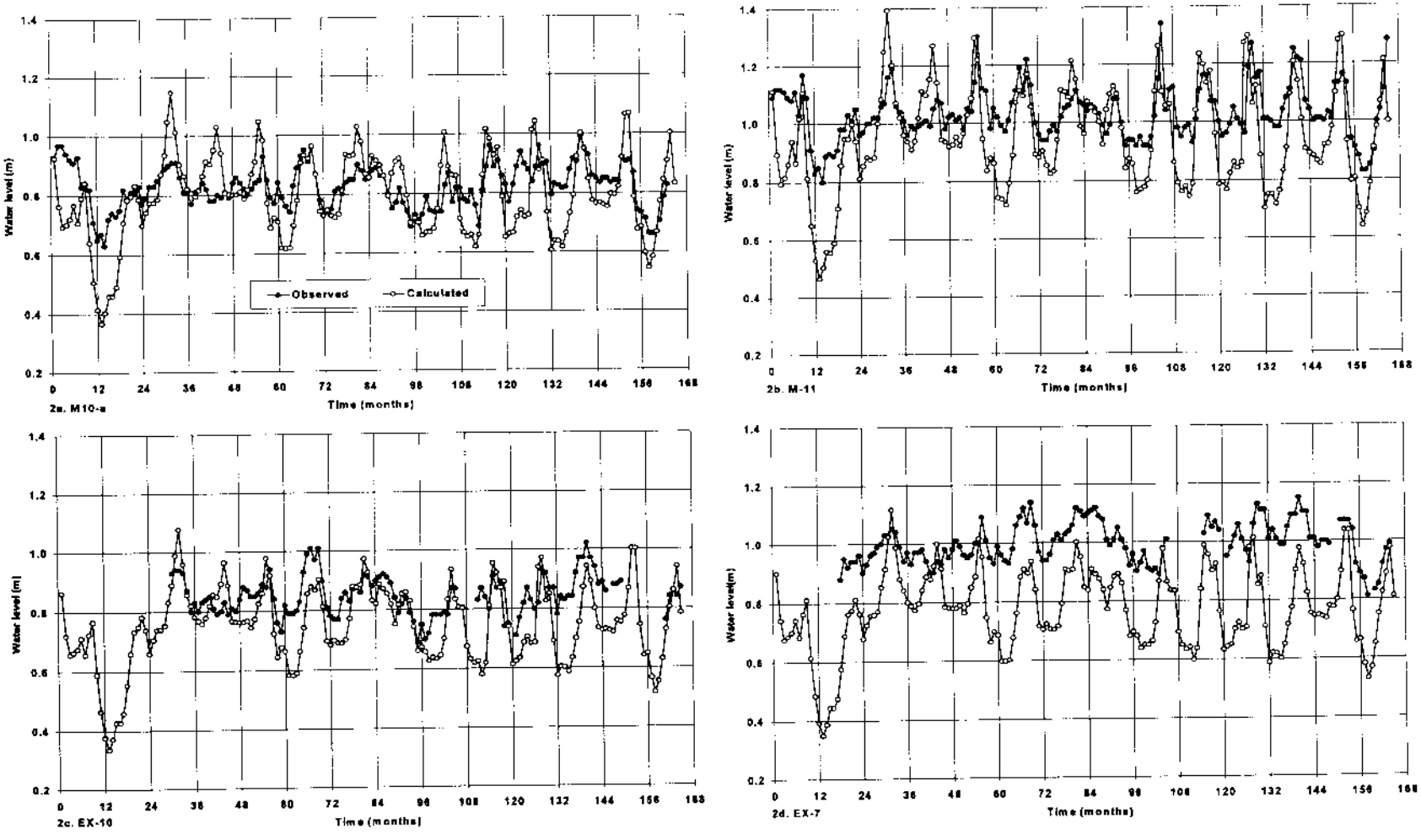

Figure 2. Simulated vs. observed mean monthly water levels for wells M-10a, M-11, Ex-10, Ex-7 for the regional best-fit value of K = 5.8 km/day from Jocson *et al.* (1999). Because their optimum was based on minimizing the overall root-mean-square error for all four wells for a single value of K applied across the entire domain, the fit at each well is not necessarily the closest that could have been obtained had the fit been optimized separately at each well. To have obtained a local best-fit for each well, however, would have required arbitrary adjustment of either the hydraulic conductivity or recharge in the vicinity of each well. The simulated curve for well M-10a (2a) is fairly well centered with respect to the observed curve. For well M-11 (2b) and Ex-10 (2c) the maxima of the curves are somewhat more closely matched in general than the minima. It is notable that at the combined optimum value for K, the simulated and observed curves for Ex-7 still exhibit an anomalous mismatch when compared with those for the other three wells, even though it is in close geographical proximity to M-10a and M-11 (Figure 1). Note that the temporal distribution of the errors is uneven—the match of the curves for some years is distinctly better than for others. The characteristic that is consistent across all four wells, however, is that amplitude of the simulated curves generally exceeds the amplitude of the corresponding observed curve.

Field observations of the NGLA reveal that flow through the vadose zone is complex (*cf.* Jenson *et al.*, 1997). A dye trace study conducted on northern Guam following Typhoon Omar in 1992 (Barner, 1995), revealed horizontal transport rates in the vadose zone of 10-100 m/day along pathways consistent with principal fracture orientations. Hydrographic observations of the water levels in observation wells (Jocson, 1998; Jocson *et al.*, 1999) have shown that when wet conditions have prevailed for at least several previous weeks, storm water from heavy rainfall can reach the water table in a matter of hours (possibly less time). This is true despite the large thickness (60-180 meters) of the vadose zone. Comparable rainfall under dry conditions, on the other hand, does not affect water table responses immediately. These observations suggest that in spite of the thin soil and high porosity of the vadose zone, it is nevertheless capable of significant storage, and that infiltration rates are dependent on the water content of at least some portion of it.

The specific characteristics or even the components of the vadose zone that could account for such storage capacity, and the processes by which the vadose zone affects infiltration rates and pathways remain unknown, however. There are no empirical data on the regional-scale storage characteristics of the epikarst or vadose bedrock beneath the epikarst, and the large scale of heterogeneity of the porosity in karst terrain makes experimental quantification from field measurements impractical. For the study reported here, we thus assumed a homogeneous vadose zone; *i.e.*, we treated the entire vadose zone as having uniform hydrologic properties, without attempting to resolve different roles for the soil layer, epikarst, or bedrock. Infiltration was assumed to be entirely vertical (which we deemed to be appropriate for the regional scale of the modeled domain). Infiltration rates were assumed, because of the evidence cited above, to reflect two separate processes: rapid infiltration through relatively open pathways fed by closed depressions in the karst surface, and slow infiltration by diffuse transport through the soil, epikarst, and bedrock matrix.

3. Parameterization of vadose characteristics

Water content and the pressure in the vadose environment are related to one another in a highly nonlinear manner. Various models have been proposed for this relationship (*e.g.*, Russo, 1988; van Genuchten and Nielson, 1985; Yeh and Harvey, 1990). We chose the van Genuchten model for this study, modifying it by the addition of a parameter, *SINK*, to account for the rapid infiltration of storm water. Rainfall that falls on the surface of the plateau is thus assumed to either evaporate, transpire or infiltrate into the vadose zone by either rapid, concentrated infiltration down open pathways, or by diffuse infiltration through the pores of the vadose zone matrix. The fraction of rainfall that travels down to the lens almost instantaneously is represented by the parameter, *SINK*. The van Genuchten parameters α, n, θ_s, θ_r, and K_s model the rest of the infiltration (1.0-*SINK*).

$$S = 1,\ h \geq 0 \qquad (1)$$

$$S = \left[1 + (\alpha|h|)^n\right]^{-\gamma_k},\ h < 0 \qquad (2)$$

$$S = (\theta - \theta_r)/(\theta_s - \theta_r) \qquad (3)$$

$$K = K_s\sqrt{S}\left[1 - \left(1 - S^{\gamma_1}\right)^{\gamma_k}\right]^2 \qquad (4)$$

Where $\gamma_k = 1 - 1/n$ and $\gamma_1 = 1/\gamma_k$,
S = effective saturation,
θ = volumetric water content (vol. of water/vol. of aquifer material),
θ_s, θ_r = saturated and residual values of θ,
K, K_s = unsaturated and saturated hydraulic conductivities,
h = soil water pressure head, and
α, n (>1) are soil material parameters, which are inversely related to the air entry value of h and the width of the soil pore size distribution, respectively.

Although vadose water retention is known to exhibit hysteretic dependence on wet-dry cycles (*cf.* Lehmann *et al.*, 1998) we do not include hysteresis effects in our model. On northern Guam, the vadose zone consists mostly of 60-180 m of karstic limestone. Diurnal or other short-term wet-dry cycles in soil moisture conditions are unlikely to have significant implications for vadose infiltration because the soil is characteristically thin and discontinuous, seldom more than a few centimeters thick, with patches of epikarst frequently exposed. For the karstic bedrock section, seasonal variations in water retention are significant (Jocson *et al.*, 1999), but perturbations in overall infiltration rates are likely to be much more strongly dependent on variations in the amount of water infiltrating by direct, rather than porous, pathways—which we account for in this model. Attempting to account for hysteresis effects would have added great complexity for only marginal improvement in accuracy.

In applications to terrain for which laboratory tests of aquifer materials can provide suitable estimates of field properties, the unsaturated soil parameters: α, n, θ_s and θ_r are typically evaluated experimentally (Hornung, 1983). Since empirical evaluation of the parameters is not practical for our application, we used values obtained by optimizing the entire parameter set so as to obtain the best fit between simulated and observed water levels. Estimates of the parameter values from field studies would presumably provide an estimate of the actual influence of the vadose zone on recharge rates. The current approach provides a means of estimating the *maximum* extent that the vadose zone *could* contribute to the explanation of the discrepancies between the observed water levels and the water levels obtained from any simulation models that exclude vadose control on recharge rates.

Many optimization models have been reported in the technical literature, some geared especially to hydrologic models. Global optimization within a feasible space is a desirable approach for hydrologic modeling, because local optima may be substantially different than the global optimum. One of the more recent models that satisfies these conditions is the Shuffled Complex Evolution (SCE-UA) Method developed at the University of Arizona (Duan, 1991; Duan *et al.*, 1993; Duan *et al.*, 1992). This model was used to optimize the six parameters, *SINK*, α, n, θ_s, θ_r, and K_s, so as to minimize the sum of the squares of the errors at four observation wells over the period 1982-1995. The error is defined as the difference between the monthly-averaged simulated and observed elevations of the water in the wells. The assigned feasible space and optimum parametric values obtained are given in Table 1.

Table 1. Optimized parameters for vadose zone.

Parameter	Assigned feasible space	Optimum value
SINK	0.0-0.50	0.325
α	0.0328-0.623 m^{-1}	0.4517 m^{-1}
n	0.01-3.0	1.393
θ_s	0.05-0.99	0.23
θ_r	0.01-0.05	0.0145
K_s	0.00305-0.0701 m/s or 264-6,057 m/day	0.00582 m/s or 503 m/day

The magnitude of the optimized value of *SINK*, 32.5%, is striking but not unreasonable given that at least 20% of the rainfall on Guam arrives in daily increments of 5 cm (2 in.) to 20 cm (7.87 in.) or greater (Jocson *et al.*, 1999). Ponding of rainfall for more than a day is seldom observed even after the heaviest storms, and there are no surface streams on the plateau to carry away runoff.

The optimum porosity of the vadose zone, θ_s, of 0.23 is within the range (.15-.25) estimated by Ayers and Clayshulte (1984) from their study of field evidence and core samples. It

is also close to the porosity (0.25) inferred for the saturated lens by Contractor and Srivastava (Contractor and Srivastava, 1990) in their saltwater intrusion study. Given this porosity, 0.23, a vadose zone of 152.4 m (500 feet) depth is capable of storing 3.51 m (138 inches) of rainfall at 10% saturation. This is equivalent to 1.38 times the average annual rainfall on Guam. Such storage is, of course, dynamic and transient; it continually drains under gravity to the lens.

The unsaturated hydraulic conductivity, K, controls the rate at which water seeps downward. The unsaturated conductivity is, of course, influenced by the unsaturated water content. In Figure 3, Equations (2) and (4) are used to calculate unsaturated water content, θ, and unsaturated hydraulic conductivity, K, as a function of the pressure head, h, based on the optimized parameters in Table 1. It can be seen that θ decreases quite gradually with decreasing h, while the value of K drops off rapidly with decreasing h.

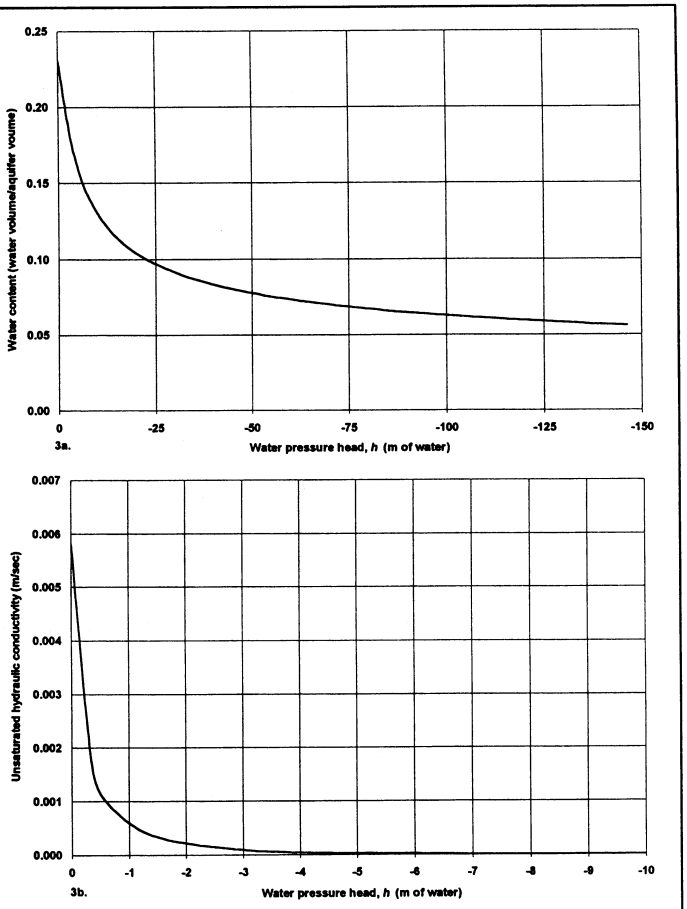

Figure 3. (a) Unsaturated water content, θ, for the optimized parameters in Table 1. (b) Unsaturated hydraulic conductivity, K, for the optimized parameters in Table 1.

4. Modeling the vadose zone using UNSAT1D

The pressure-head form of the differential equation describing one-dimensional, vertical flow of water in an unsaturated, homogenous and isotropic porous medium is

$$\frac{\partial}{\partial z}\left[K_{(h)}\frac{\partial}{\partial z}(h-z)\right]=C_{(h)}\frac{\partial h}{\partial t} \qquad (5)$$

where $K_{(h)}$ is the unsaturated hydraulic conductivity; $C_{(h)}$ is the specific water capacity, $\partial\theta/\partial h$; z is the vertical coordinate (positive downwards); and t is time. A fully documented, Galerkin, finite element FORTRAN program, UNSAT1D, has been developed by Khaleel and Yeh (1985) to solve Equation (5). The domain is discretized with linear line elements. A variable time is used step to keep the error below a specified tolerance. Material-balance error summaries are presented at each time step to document the accuracy of the numerical scheme.

We applied UNSAT1D in this study to model the infiltration of rainfall excess through the vadose zone above the freshwater lens in the NGLA. We deemed a one-dimensional model to be appropriate for our application since infiltration is assumed to be generally vertical at the scale of the model. Moreover, data on vadose pathways in the bedrock are insufficient to support a higher-dimensional model. To account for the variation in thickness of the vadose zone across the domain of the SWIG2D model, we assigned a separate vadose column above each element in

the SWIG2D domain, the depth of which was equal to the thickness of the vadose zone above sea level at the respective SWIG2D element. Each vadose column was discretized into 50 equal elements. At the upper boundary, the flow rate (rainfall excess) is specified as a function of time. The lower boundary was assumed to be at mean-sea-level (MSL) and the head is specified as zero. The phreatic surface of the aquifer is about 1 m (3-4 ft.) above MSL, but this is small compared to the thickness of the vadose zone, which can be 30-150 m (100-500 ft.). The program calculates the head at all the nodes and the flow rate at the bottom of the vadose zone, which is the recharge to the lens. The recharge is then input to the phreatic model (SWIG2D) to calculate the response of the phreatic zone.

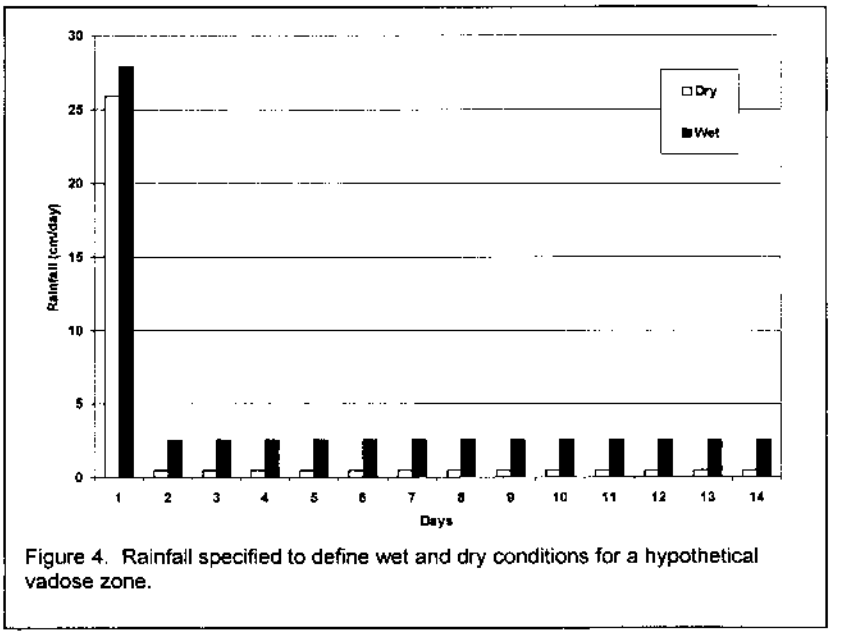

Figure 4. Rainfall specified to define wet and dry conditions for a hypothetical vadose zone.

5. Simulations

5.1 Hypothetical applications

The first application of UNSAT1D is to a hypothetical vadose zone, 152.4 m (500 feet) thick, having the characteristics shown in Table 1. The purpose of this application is to simulate the general response of the simulated vadose zone to a concentrated impulse of rainfall excess at the top. The response of the vadose zone depends on how wet or dry it is. Two cases are examined. The first is a dry vadose zone, in which 5.08 mm (0.2 inches) of rainfall excess occurs daily. The second is a wet vadose zone, in which 25.4 mm (1.0 inch) of rainfall excess occurs daily. Each of these cases is subjected to an impulse of 25.4 cm (10 inches) of rainfall on day 1 (Figure 4).

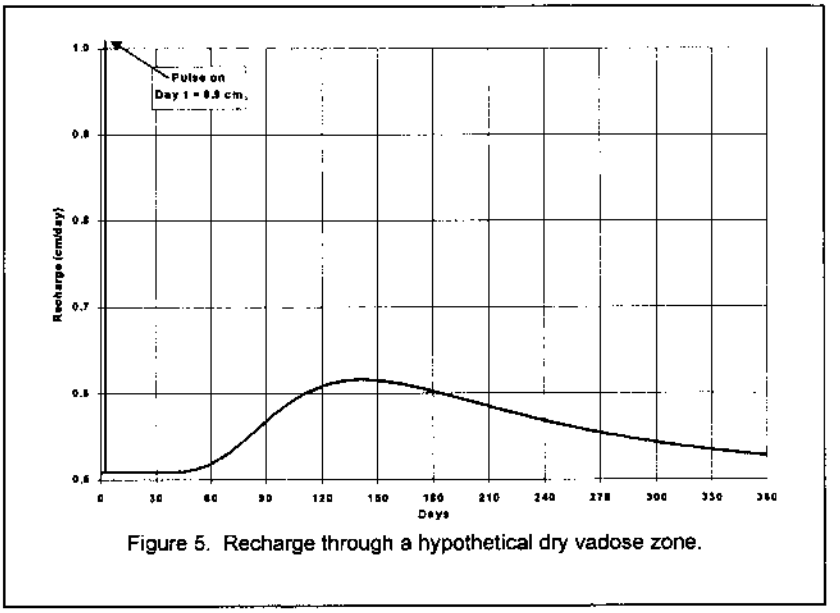

Figure 5. Recharge through a hypothetical dry vadose zone.

UNSAT1D was run for these two cases to obtain the recharge at the bottom of the vadose zone as a function of time. The initial conditions for the two cases were obtained by simulating the background rainfall (5.08 mm and 25.4 mm) for a sufficiently long time, until steady state

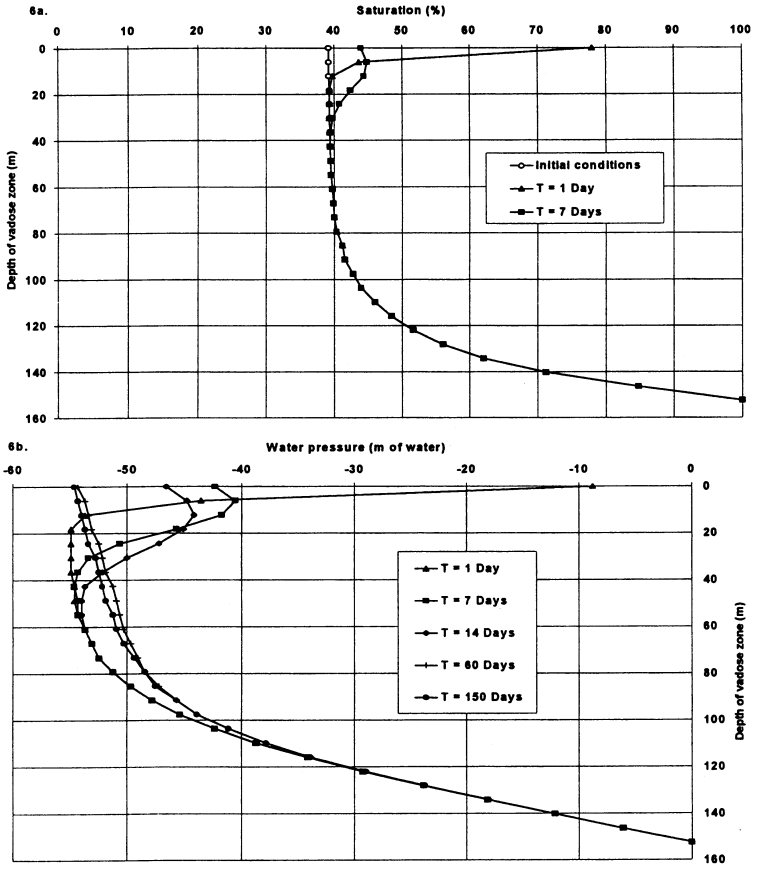

Figure 6. Calculated profiles for (a) water content, θ, and (b) water pressure, h, in a hypothetical dry vadose zone.

conditions were obtained. After many trials, it was determined that the maximum time step, Δt, that could be specified without inducing convergence and stability problems was Δt = 1 day. Figure 5 shows the recharge to the lens for the dry vadose case. The recharge due to the impulse of 25.4 cm (10 inches) on day 1 appears on top of the background influx, producing the spike on day 1, which also reflects the effect of the parameter, *SINK*. Since 25.4 cm (10 inches) of rainfall excess fell on day 1 and *SINK* is equal to 32.5%, the recharge is equal to 8.255 cm (3.25 inches) above the background level of 5.08 mm (0.2 inches). The rest of the rainfall seeps through the vadose zone and two months later just begins to appear at the lens. The peak recharge occurs about 5 months after the rainfall; even a year after the rainfall, the recharge is not complete. Figure 5 shows that rainfall takes a long time to infiltrate through a dry vadose zone via the diffuse pathway. The travel time would be proportionately shorter for a thinner vadose zone. If the vadose zone were drier, the travel times would be longer.

Figure 6a shows the profiles of water content in the dry vadose zone at different times. The initial condition is shown along with the change at the end of Day 1 and Day 7. It can be seen that 25.4 cm (10 inches) of rainfall causes only small changes in the water content of the vadose zone. Figure 6b shows the changes in the pressure head, h, of the water in the vadose zone at different times after the rainfall. Figure 6 shows why it is important to have the correct initial conditions when simulating a vadose zone. An incorrect initial pressure-head distribution can produce very erroneous results, even sufficient to generate instabilities and non-convergence in the program.

Figure 7 shows the recharge to the lens through a hypothetical wet vadose zone of the same thickness, subject to the same initial impulse of rainfall. Note that the travel times are much shorter than for the dry vadose zone (Figure 5). Note that the peak recharge occurs in 2 months and that the recharge event is complete in 6 months. If the vadose zone were wetter, the travel times would be even shorter. A striking similarity occurs between the response of the vadose zone to an impulse of rainfall excess and the hydrograph response of a watershed to an impulse of rainfall in surface hydrology. When the impulse of rainfall excess is reduced to one-half (*i.e.* to 12.7 cm (5 inches)), the response peak is reduced to one-half of the peak shown in Figure 7, while the time-to-peak remains unchanged.

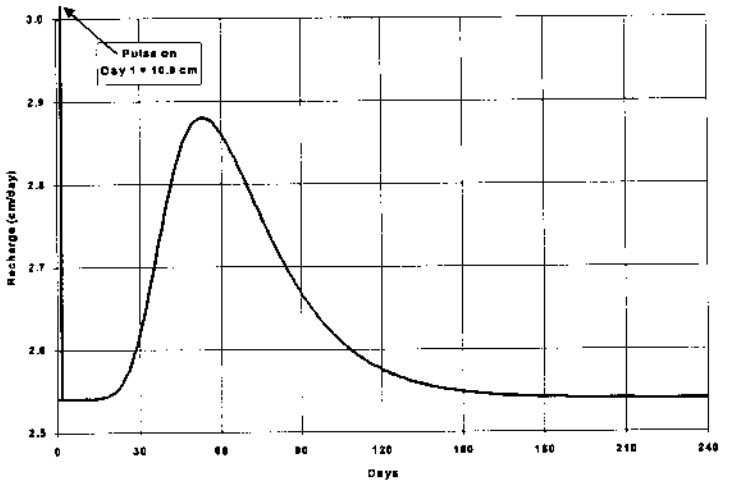

Figure 7. Recharge through a hypothetical wet vadose zone.

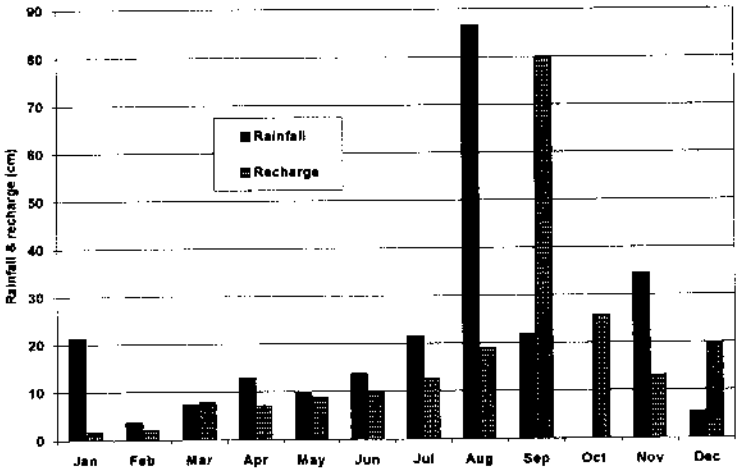

Figure 8. Effect of hypothetical vadose zone on monthly recharge for rainfall data from 1992 (NAS rain gage, Agana).

UNSAT1D was next applied to a hypothetical vadose zone 152.4 m (500 feet) thick, subjected to the measured monthly-averaged values of rainfall excess recorded for Guam at the NAS gage station (Figure 1) in 1992. Figure 8 shows the rainfall excess (input) and calculated recharge (output) for each month. Note that the heavy rainfall in August (associated with the passage of Typhoon Omar, 28-29 Aug 1992) appears as recharge in September and even partially in October, for which zero rainfall excess was input to the model. (In specifying zero rainfall excess for October, we attempted to make a virtue of necessity: No data were collected at the NAS rain gage during October 1992 because the gage was out of service for that month. Applying the zero value for October, however, allows the model to calculate a minimum recharge value for October, based solely on the recharge of the previous months.)

The results of these simulations for specified hypothetical conditions are realistic and within the range of responses that seem reasonable for the NGLA. They therefore provide some confidence that our modifications to UNSAT1D was free of programming errors or other errors of implementation, and that the vadose model is appropriate for application to the question posed in this study.

5.2 Application to the NGLA

UNSAT1D was next coupled to a phreatic model of a selected sub-basin of the NGLA. We selected the Yigo-Tumon and Finegayen sub-basins (Figure 1), because a successful SWIG2D-based phreatic model of them was already available (Jocson, 1998; Jocson *et al.*, 1999) and active. The Yigo-Tumon sub-basin is also the largest, most economically important, and well-documented of the aquifer's six sub-basins. The Finegayen sub-basin is adjacent to it and is undergoing the most active production development at the current time. The 95-km^2 domain of

the phreatic model was discretized into 1057 triangular elements, with 579 nodes, for use by the SWIG2D-based phreatic model. Figure 9 shows the finite element network. The northern and southern boundaries are no-flux boundaries. The eastern boundary is a freshwater flux boundary. Rainfall excess infiltrates through the neighboring limestone to the volcanic basement and then flows laterally at mean-sea-level through 56 element boundaries into the lens. The western boundary is a coastal boundary. At 32 coastal nodes, the saltwater head was specified according to measured sea-level data, mainly from the Agana tide gage (Figure 1). There are 48 production wells that withdraw groundwater. Because the actual wells do not always coincide with nodes, the production was distributed over 52 nodes. Production did not vary significantly on a monthly basis.

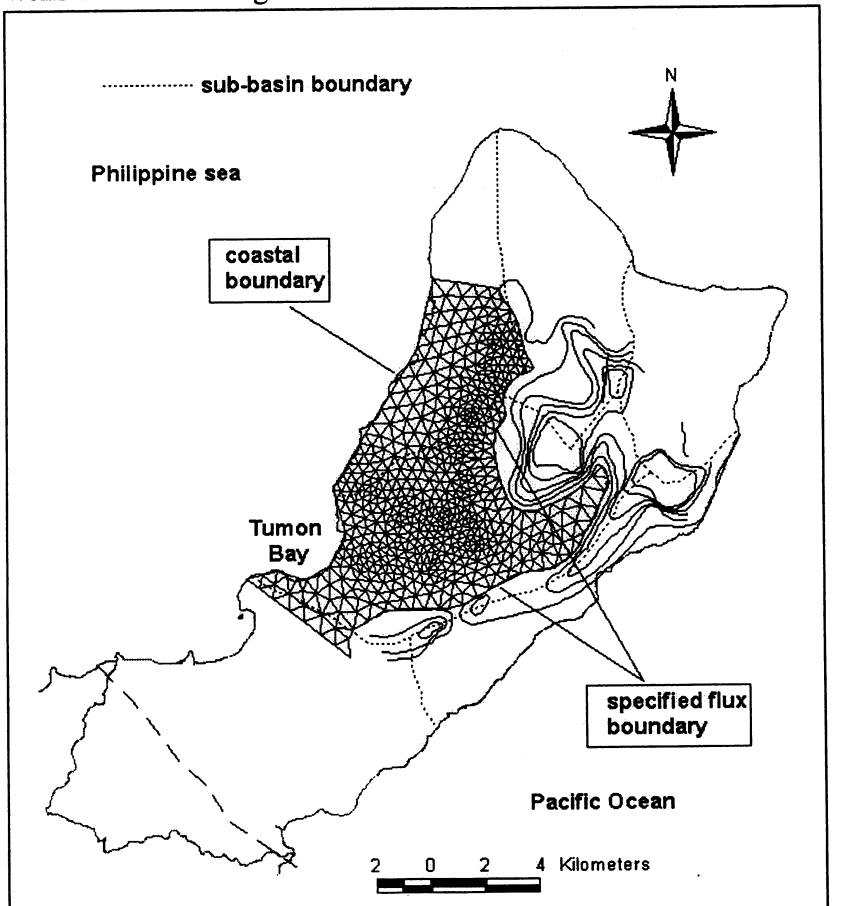

Figure 9. Finite element domain for the SWIG2D-based model of the freshwater lens.

Although UNSAT1D can calculate daily recharge values, the phreatic model required a time step of 1 month. Hence, we input monthly-averaged values of rainfall excess to UNSAT1D. Monthly rainfall excess was defined as the monthly total of the positive-definite differences between daily rainfall minus daily pan evaporation (thus estimating maximum evapotranspiration, hence minimum recharge) (Jocson, 1998; Jocson *et al.*, 1999). For control purposes, porosity of the phreatic zone was assigned to be 0.23, the same assigned to the vadose zone. Before coupling the phreatic and vadose models, we repeated the parametric sensitivity analyses conducted by Jocson (1998). He had parameterized the SWIG2D model to obtain a constant value of the regional hydraulic conductivity that would minimize the errors between the calculated and measured water levels at four wells in the absence of vadose infiltration. The resulting conductivity of 5.8 km/day (19,000 ft/day) produced the best-fit results (shown earlier in Figure 2) that can be obtained when the vadose zone is ignored and recharge to the lens is assumed to occur "instantaneously," *i.e.*, within each monthly time step. Inspection of Figure 2 shows that a significant—and systematic—mismatch between the observed and simulated curves remains even after hydraulic conductivity is optimized.

6. Combining UNSAT1D, SWIG2D, and SCE-UA

The two programs, UNSAT1D and SWIG2D, were combined into a single program, VADOSWIG (Figure 10), so that well water levels could be calculated directly from rainfall in a single execution. VADOSWIG calls three subroutines to obtain the computed well water levels. The first, SUBRVADO, is a copy of UNSAT1D that calculates recharge from water infiltrating directly to the lens (and thus internal to the domain of the phreatic model) and passes it to SUBRSWIG, which is a copy of SWIG2D. The subroutine SUBVADO2 is also a copy of UNSAT1D. This subroutine calculates the recharge arriving on the flank of the basement between the eastern boundary of the finite element network and the subterranean basement hydrologic divide (thus external to the domain of the phreatic model). The rainfall excess that occurs over this area is assumed to infiltrate vertically through the vadose zone to the volcanic basement and then along the topographic gradient of the basement to enter the lens as a freshwater boundary flux. Hence, the output of SUBVADO2 provides the freshwater boundary flux to subroutine SUBRSWIG. With the outputs from SUBRVADO and SUBVADO2, SUBRSWIG calculates the heads, lens thickness, and velocities at each node in the FEM network. SUBRSWIG also calculates the sum of the squared errors at the observation wells. After each run of VADOSWIG, the optimization routine is invoked to optimize the vadose parameters by minimizing the objective function. SCEMAIN controls the optimization, taking the objective function and specified feasibility space from SCEIN, and passing them to the optimization subroutine, which is a copy of SCE-UA.

Because the thickness of the overlying vadose zone varies from element to element in the two-dimensional phreatic model, and each of the elements of the phreatic model has a different rainfall excess at the top of the vadose column, we initially had to execute the UNSAT1D program 1057 times to calculate unique recharge values for each element. Hence, a single execution of VADOSWIG on a 300 MHz Pentium II computer took about 6 hours. While this was tolerable for a single run, it is clearly too long for iterations within an optimization program. To reduce the execution time of UNSAT1D, we used a monthly-mean value of the rainfall excess instead of a diurnally variable value for each element. We also specified the elevation of the vadose zone by the use of the nearest-contour method (using 30.5-m or 100-ft intervals) rather than by interpolation. This technique reduced the number of runs for UNSAT1D from 1057 to 5, because the elements had vadose thicknesses of 30, 60, 90, 120, and 150 m (100, 200, 300, 400 or 500 ft.). These two modifications reduced the execution time for VADOSWIG from 6 hours to 7 minutes. The reduced execution time made it practical to couple the SCE-UA program with VADOSWIG

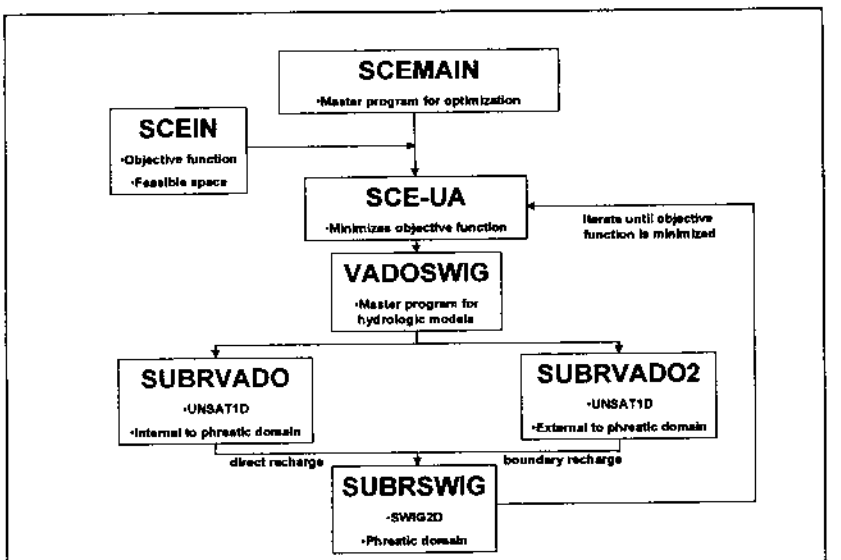

Figure 10. Schematic flow chart of the structure of the master program integrating the vadose model, the phreatic model, and the optimization algorithm. Details are described in the text.

(Figure 10). VADOSWIG could then be run for each evaluation of the objective function required by SCE-UA.

7. Results and Discussion

Table 2 shows the percent reduction in error in each of the four wells achieved by coupling the vadose model to the phreatic model. The total sum-of-squared-errors (SSE) for the no-vadose-zone case was 14.458 m^2. The SSE with the optimized vadose zone included is 10.202 m^2, a reduction in SSE of 29.4%. Figure 11 shows the comparison of observed and computed water levels in the four observation wells in the sub-basin when vadose infiltration is simulated. Comparison of Figure 11 with Figure 2 shows that the differences between the peak and low water levels are in general reduced in the simulation from the coupled model compared with the levels from the model excluding vadose processes. In Figure 12, the simulated water level responses from Figures 2 and Figure 11 are overlain for well M-11.

Table 2. Error reduction with simulation of vadose zone.
(SSE in meters)

Well number	Without vadose zone	With vadose zone	Percent reduction
M-10a	2.217	0.984	55.6
M-11	4.020	2.237	44.4
EX-10	1.566	1.042	33.5
EX-7	6.655	5.939	10.8
TOTAL	14.458	10.202	29.4

Figure 13 compares the responses when rainfall excess is averaged over the aquifer versus when it is varied by interpolation over every element of the network. It can be seen that the results are not strongly sensitive to the approximation. Hence, optimization with the rainfall excess and elevation varying from element to element would have resulted in virtually the same optimal values and SSE, at the expense of an enormous penalty in extended execution time.

Figure 14 shows the simulated water content profiles in a hypothetical 152.4-m (500-ft.) thick vadose zone for historically representative dry and wet conditions. In May 1983 (an El Nino year), the vadose zone was very dry due to very low rainfall excess in the previous months. In August 1985, the vadose zone was very wet due to heavy rainfall excess in the previous months. The water-content profiles show changes in the upper part of the simulated vadose zone. The lower part of the vadose zone is influenced by the lower boundary condition, where saturated conditions prevail.

Finally, the depth of the interface computed by the model is compared with the depth of the 50% isochlor measured in observation well Ex-10 (Figure 15). The computed depths are given when the vadose zone is omitted and included. The differences between the two are quite small. Note that the measured depth of the interface is greater than the depths of both of the computed curves and hence the model predicts a conservative depth to the interface. The root-mean-square error is 8.01 m or about 23% of the observed depth to the 50% isochlor. The cause of this discrepancy has not been determined, but may reflect stratigraphic variations in the horizontal hydraulic conductivity of the phreatic zone in the vertical direction (perhaps associated with the complex sea-level history of the island), which are not accounted for in this two-dimensional model.

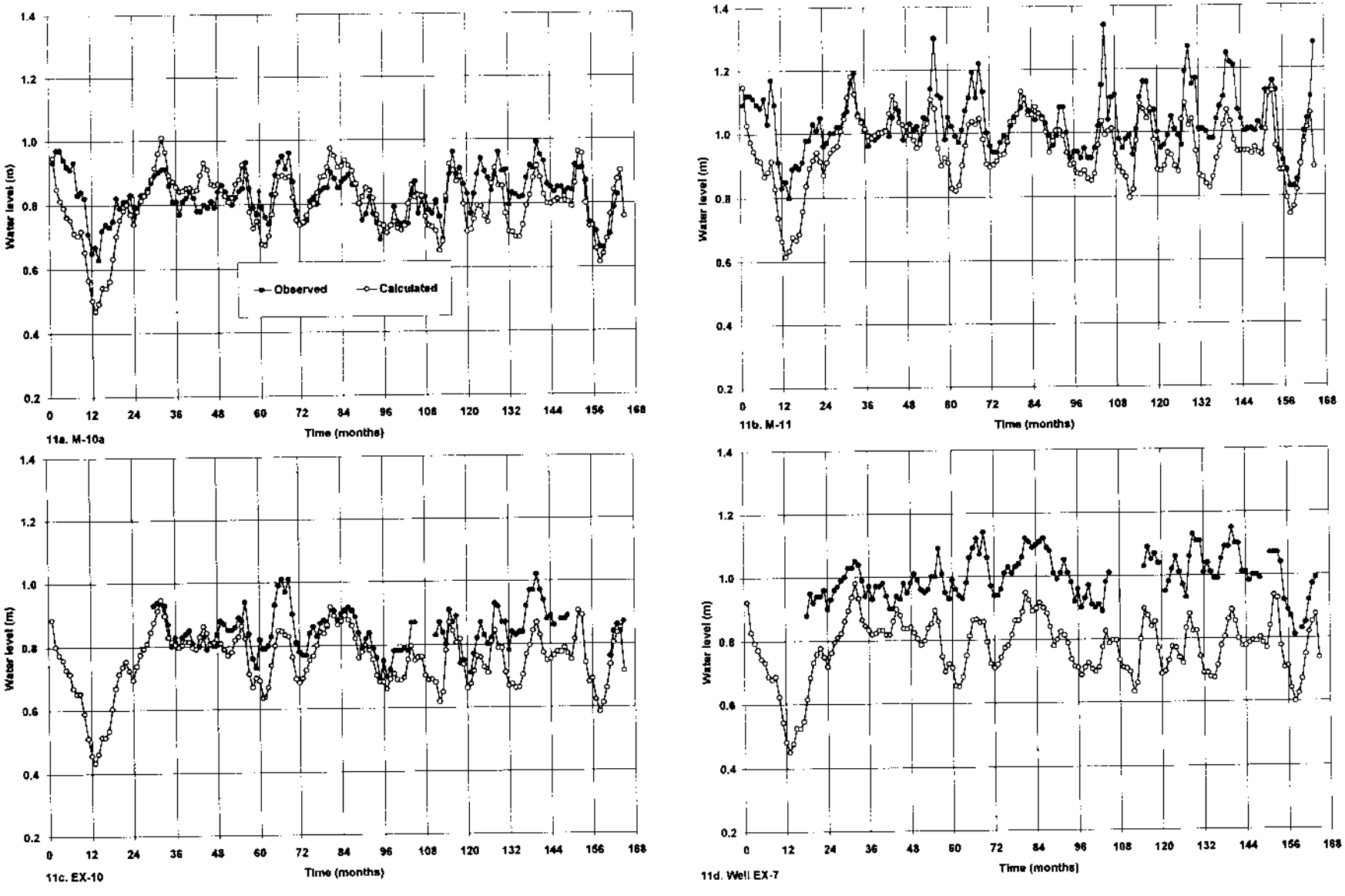

Figure 11. Comparison of observed well levels with simulations incorporating the vadose model for wells M-10a, M-11, Ex-10, Ex-7. (Compare Figure 2.)

8. Conclusions

The results of the study reported here are consistent with the hypothesis that temporary storage of infiltrating water in the vadose is significant and infiltration rates are strongly dependent on the water content of the vadose zone of the Northern Guam Lens Aquifer. The optimized values of the vadose parameters seem reasonable for the geology of the aquifer and are consistent with values derived by other means in previous studies. Optimizing the vadose parameters reduced the total SSE between measured and computed water levels in four observation wells from 14.458 m^2 to 10.202 m^2, a reduction of 29.4%. A 30% reduction in the SSE suggests a significant role for the vadose zone, in the hydrology of the aquifer. The fact that the reduction was not more than 30%, suggests that temporal and spatial variations in vadose zone characteristics are insufficiently known and/or that other processes affecting the temporal and spatial distribution of recharge have yet to be incorporated.

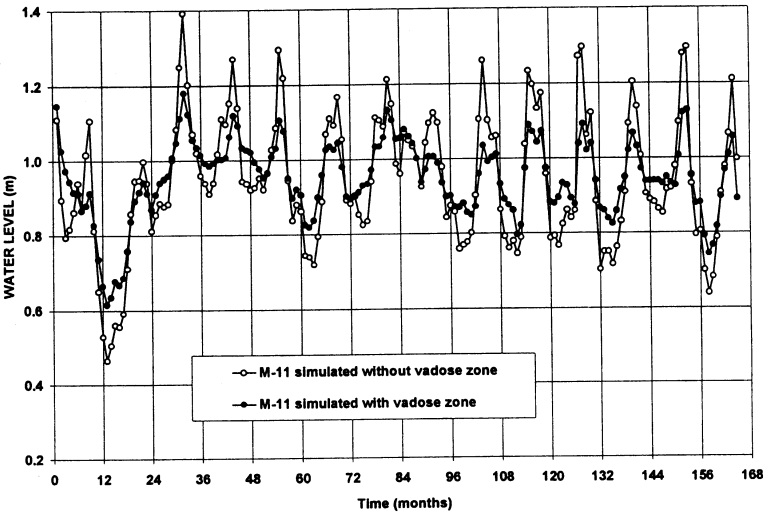

Figure 12. Comparison of simulated water levels for M-11 with and without the vadose model included.

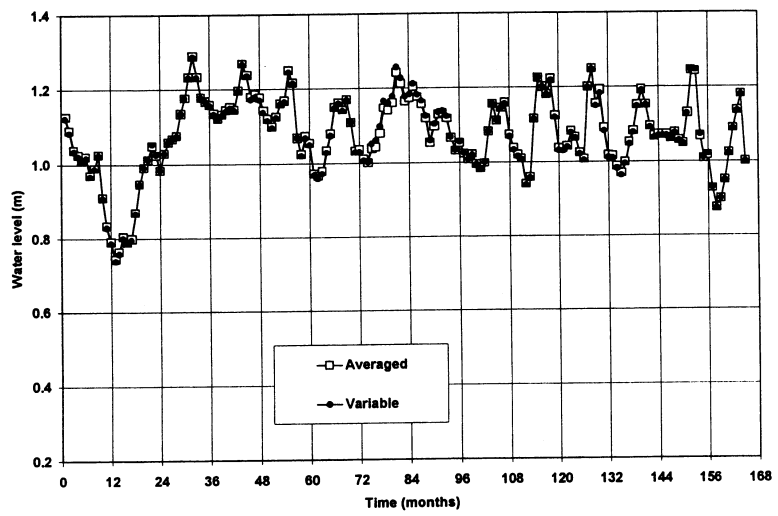

Figure 13. Comparison of simulation results for rainfall excess averaged over the aquifer versus rainfall excess varied by interpolation over every element, well M-11.

An obvious source of error excluded in this study as well as previous modeling studies is the spatial variability of the hydraulic conductivity in the aquifer. Unfortunately, the data are still insufficient to resolve separate values of conductivity for individual elements in the phreatic model. There are no empirical data at all, upon which to base estimates of the magnitude or variation in vadose conductivity. A second source of error is variation in evapotranspiration, both spatial and temporal. Very little is known about the dependence of water loss (soil moisture) due to vegetation on Guam. Evapotranspiration is probably the dominant determinant of water loss when light rainfall occurs during dry conditions, but when the soil layer is at or near saturation, evapotranspiration is probably not a significant determinant of infiltration. A third, and probably

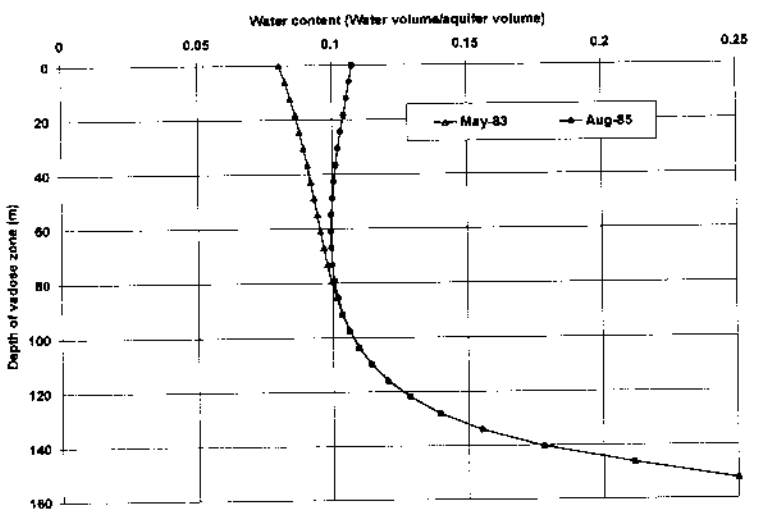

Figure 14. Hypothetical water content profiles for historically dry (May 1983) and wet (August 1986) conditions.

more significant source of error, especially under wet conditions, might be the dependency of infiltration and storage on precipitation rates on Guam. That the optimized value of the rapid- infiltration parameter, *SINK*, was 32.5% suggests that rapid, ephemeral flow through the aquifer is important. On the other hand, it seems reasonable to infer that the actual value of this parameter may vary not only spatially as a function of the distribution of karst features on the terrain, but also be a function of the rate of precipitation. Continued modeling studies, along with statistical comparison with the historical record and field hydrographic studies, should yield additional insights into aquifer properties that can help achieve greater confidence in understanding the role of the vadose zone in determining the response of the fresh water lens.

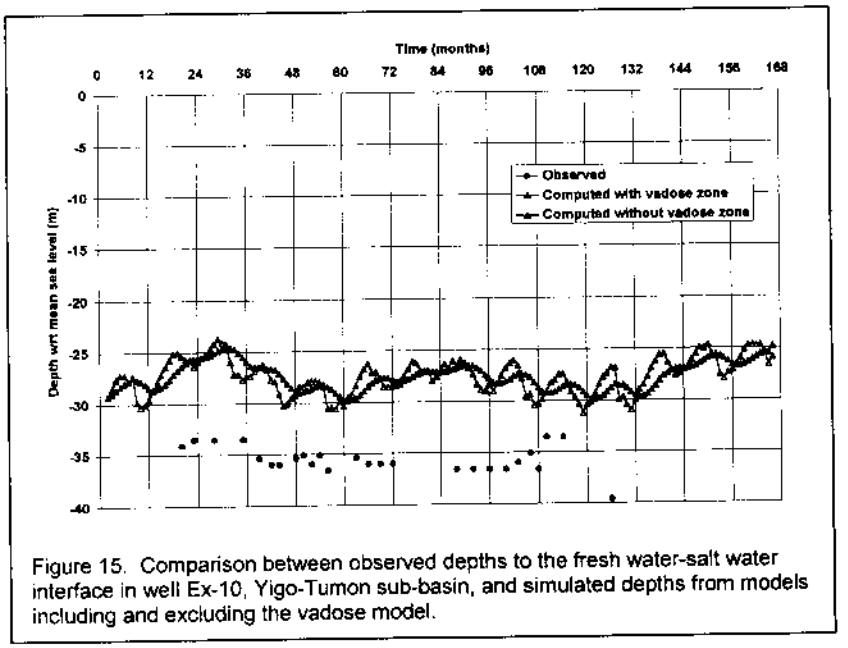

Figure 15. Comparison between observed depths to the fresh water-salt water interface in well Ex-10, Yigo-Tumon sub-basin, and simulated depths from models including and excluding the vadose model.

Acknowledgements

This study was funded through the Guam Hydrologic Survey Program, Water and Environmental Research Institute of the Western Pacific (WERI) of the University of Guam, provided by the 24th Guam Legislature on the initiative of the Committee on Natural Resources, Senator Joanne Brown, Chair. D.N. Contractor spent his sabbatical leave at WERI and is grateful to H.G. Siegrist, J.W. Jenson, and J.M.U. Jocson for their support. Thoughtful reviews of the manuscript by Ling Li and H. Leonard Vacher significantly improved the final paper.

Appendix

SWIG2D is a two-dimensional, linear-triangle finite element, dual-phase/sharp interface, Darcian/Dupuit groundwater program (Contractor and Srivastava, 1990). The depth-averaged differential equations for fresh water and salt water implemented in the code were derived by Sa Da Costa and Wilson (1979):

Fresh water:

$$\frac{\partial}{\partial x_i}\left(K_{ij}^f b^f \frac{\partial h^f}{x_j}\right) + N + q_p^f = \left(S^f + \frac{\eta\gamma^f}{\Delta\gamma}\right)\frac{\partial h^f}{\partial t} - \frac{\eta\gamma^s}{\Delta\gamma}\frac{\partial h^s}{\partial t}$$

Salt water:

$$\frac{\partial}{\partial x_i}\left(K_{ij}^s b^s \frac{\partial h^s}{\partial x_j}\right) + q_p^s = \left(S^s + \frac{\eta\gamma^s}{\Delta\gamma}\right)\frac{\partial h^s}{\partial t} - \frac{\eta\gamma^f}{\Delta\gamma}\frac{\partial h^f}{\partial t}$$

Where b is the thickness of the fresh/salt water
h is pressure head
K is the conductivity of the aquifer
N is the recharge to the aquifer
q_p is the pumping rate
(+for recharge;-for extraction)
S is the storativity of a confined aquifer
t is time
x is the coordinate direction
γ is specific weight
η is porosity
$\Delta\gamma$ is difference in salt and fresh water specific weights
Subscripts i, j refer to coordinate directions
Superscripts. f, freshwater; s, saltwater

Anisotropic hydraulic conductivity can be parameterized by specifying K_{max} and K_{min}, the maximum and minimum conductivities, and θ, the angle of K_{max} from the abscissa. The code computes and uses the component terms of the conductivity tensor:

$$K_{xx} = K_{max}\cos^2\theta + K_{min}\sin^2\theta$$

$$K_{yy} = K_{max}\sin^2\theta + K_{min}\cos^2\theta$$

$$K_{xy} = K_{yx} = (K_{max} - K_{min})\sin\theta\cos\theta$$

The code has been configured for either transient or steady-state problems. Dirichlet and Neuman type boundary conditions can be specified. Coastal boundaries can be simulated using a mixed (Cauchy) boundary condition. Pumps for either salt water or fresh water can be specified at any node of the network. Output includes fresh water and salt water heads, lens thickness at each node, and the mean groundwater velocity for each element. The current version of SWIG2D uses a pre-programmed package (Kincaid *et al.*, 1997) for solving large, sparse, linear systems by

adaptive, accelerated, iterative methods. This feature allows the nodes in the network to be numbered in any sequence, without a penalty in increased memory requirement or execution time resulting from increased bandwidths, which is particularly advantageous when modifying existing networks.

References

Ayers, J.F. and Clayshulte, R.N., 1984. A preliminary study of the hydrogeology of northern Guam. Technical Report #56, Water & Energy Research Institute of the Western Pacific, University of Guam, Mangilao.

Barner, W.L., 1995. Ground water flow in a young karst terrane developed along a coastal setting, northern Guam, Mariana Islands, Int. Res. Appl. Cen. Karst Water Res., Karst Waters Institute, Seminar field course, Beldibi/Antalya, Turkey, pp. 12.

CDM, 1982. Final Report, Northern Guam Lens Study, Groundwater Management Program, Aquifer Yield Report, Camp, Dresser and McKee, Inc. in assoc. with Barrett, Harris & Associates for Guam Environmental Protection Agency.

Contractor, D.N., 1981. A two-dimensional, finite-element model of salt water intrusion in groundwater systems. Technical Report #26, Water and Energy Research Institute of the Western Pacific, University of Guam, Mangilao.

Contractor, D.N., 1983. Numerical modeling of saltwater intrusion in the Northern Guam Lens. Water Resources Bulletin, 19: 745-751.

Contractor, D.N., Ayers, J.F. and Winter, S.J., 1981. Numerical modeling of salt-water intrusion in the Northern Guam Lens. Technical Report #27, Water and Energy Research Institute of the Western Pacific, University of Guam, Mangilao.

Contractor, D.N. and Srivastava, R., 1990. Simulation of saltwater intrusion in the Northern Guam Lens using a microcomputer. Journal of Hydrology, 118: 87-106.

Duan, Q., 1991. A Global Optimization Strategy for Efficient and Effective Calibration of Hydrologic Models. Ph.D. Dissertation, University of Arizona, Tucson.

Duan, Q., Gupta, V.K. and Sorooshian, S., 1993. A Shuffled Complex Evolution Approach for Effective and Efficient Global Minimization. Journal of Optimization Theory and its Application, 61(3).

Duan, Q., Sorooshian, S. and Gupta, V.K., 1992. Effective and Efficient Global Optimization for Conceptual Rainfall-Runoff Models. Water Resources Research, 28(4): 1015-1031.

Hornung, U., 1983. Identification of Non-linear Soil Physical Parameters from an Input-output Experiment. In: P. Deyufthard and E. Haier (Editors), Workshop on Numerical Treatments of Inverse Problems in Differential and Integral Equations. Birkhauser, pp. 227-237.

Jenson, J.W., Jocson, J.M.U. and Siegrist, H.G., 1997. Groundwater discharge styles from an uplifted Pleistocene island karst aquifer, Guam, Mariana Islands. In: B.F. Beck and J.B. Stephenson (Editors), The Engineering Geology and Hydrology of Karst Terranes. Balkema, Springfield, Missouri.

Jocson, J.M.U., 1998. Hydrologic model for the Yigo-Tumon and Finegayan subbasins of the Northern Guam Lens Aquifer, Guam. Masters Thesis, University of Guam, Mangilao, 95 pp.

Jocson, J.M.U., Jenson, J.W. and Contractor, D.N., 1999. Numerical Modeling and Field Investigation of Infiltration, Recharge, and Discharge in the Northern Guam Lens Aquifer. Technical Report #88, Water and Environmental Research Institute of the Western Pacific, University of Guam, Mangilao.

Khaleel, R. and Yeh, T.-C., 1985. A Galerkin Finite Element Program for Simulating Unsaturated Flow in Porous Media. Ground Water, 23: 90-96.

Kincaid, D.R., Respess, J.R., Young, D.M. and Grimes, R.G., 1997. ITPACK 2C: A FORTRAN Package for Solving Large Sparse Linear Systems by Adaptive Accelerated Iterative Methods. ACM Transactions on Mathematical Software, 8(3): 302-322.

Lehmann, P., Stauffer, F., Hinz, C., Dury, O. and Fluhler, H., 1998. Effect of Hysteresis on Water Flow in a Sand Column with a fluctuating Capillary Fringe. Jour. of Contaminant Hydrology, 33: 81-100.

Mink, J.F. and Vacher, H.L., 1997. Hydrogeology of northern Guam. In: H.L. Vacher and T. Quinn (Editors), Geology and Hydrogeology of Carbonate Islands. Developments in Sedimentology 54. Elsevier Science, Amsterdam, pp. 743-761.

Mylroie, J.E. and Vacher, H.L., 1999. A conceptual view of island karst. In: A.N. Palmer, M.V. Palmer and I.D. Sasowsky (Editors), Karst Modeling Symposium, Charlottesville, VA, pp. 48-58.

Russo, D., 1988. Determining Soil Hydraulic Properties by Parameter Estimation: On the Selection of a model for the Hydraulic Properties. Water Resources Research, 24: 453-459.

Sa da Costa, A.A.G. and Wilson, J.L., 1979. Numerical model of seawater intrusion in aquifers. 247, Massachusetts Institute of Technology Technical Report.

Tracey, J.I., Jr., Schlanger, S.O., Stark, J.T., Doan, D.B. and May, H.G., 1964. General Geology of Guam. 403-A, U.S. Geological Survey Professional Paper, US Government Printing Office, Washington, D.C.

Vacher, H.L. and Mylroie, J.E., submitted. Double Porosity of Eogenetic Karst. Geology.

van Genuchten, M.T. and Nielson, D.R., 1985. On Describing and Predicting the Hydraulic Properties of Unsaturated Soils. Ann. Geophys., 3: 615-628.

Yeh, T.-C.J. and Harvey, D.J., 1990. Effective Unsaturated Hydraulic Conductivity of Layered Soils. Water Resources Research, 26.